Lab on a Chip

RSC Publishing

PAPER

View Article Online
View Journal | View Issue

Optoacoustic tweezers: a programmable, localized cell concentrator based on opto-thermally generated, acoustically activated, surface bubbles†

Cite this: *Lab Chip*, 2013, **13**, 1772

Yuliang Xie,‡[ab] Chenglong Zhao,‡[b] Yanhui Zhao,[b] Sixing Li,[b] Joseph Rufo,[b] Shikuan Yang,[b] Feng Guo[b] and Tony Jun Huang*[ab]

Received 8th January 2013,
Accepted 28th February 2013

DOI: 10.1039/c3lc00043e

www.rsc.org/loc

We present a programmable, biocompatible technique for dynamically concentrating and patterning particles and cells in a microfluidic device. Since our technique utilizes opto-thermally generated, acoustically activated, surface bubbles, we name it ''optoacoustic tweezers''. The optoacoustic tweezers are capable of concentrating particles/cells at any prescribed locations in a microfluidic chamber without the use of permanent structures, rendering it particularly useful for the formation of flexible, complex cell patterns. Additionally, this technique has demonstrated excellent biocompatibility and can be conveniently integrated with other microfluidic units. In our experiments, micro-bubbles were generated by focusing a 405 nm diode laser onto a gold-coated glass chamber. By properly tuning the laser, we demonstrate precise control over the position and size of the generated bubbles. Acoustic waves were then applied to activate the surface bubbles, causing them to oscillate at an optimized frequency. The resulting acoustic radiation force allowed us to locally trap particles/cells, including 15 μm polystyrene beads and HeLa cells, around each bubble. Cell-adhesion tests were also conducted after cell concentrating to confirm the biocompatibility of this technique.

Introduction

A programmable cell concentrator is characterized by its ability to trap and concentrate cells at any pre-defined position, control the extent of cell aggregation, and form cell arrays consisting of multiple concentrating spots. Compared with conventional cell concentrators, which are primarily used for pretreatment of diluted cell samples, a programmable cell concentrator has more functionalities and can have broader applications, such as point-of-care diagnostics,[1,2] cell microarrays,[3,4] tissue engineering,[5] regenerative medicine,[6] and cell–cell communication pathway studies.[7,8] For instance, in diagnostic systems which involve diluted samples, concentrating target cells at predefined locations can increase local cell concentration, thus locally enhancing detection sensitivity and improving the flexibility and performance of the device.[9] The importance of controlling the extent of cell aggregation is demonstrated in the analysis of the cell contact inhibition phenomenon; in these studies, the behavior of cells which are concentrated until they come in close contact with one another is examined in order to distinguish cancerous cells from normal cells.[10] In another example, the ability to simultaneously concentrate cells at several pre-defined spots has significantly contributed to the study of cells' collaborative relations in tissue engineering,[4] in which programmable cell arrays of various configurations and separation distances allow researchers to investigate certain cell behaviors, such as cell–cell communication with extracellular signaling molecules.[7,8]

While the significance of an on-chip, programmable cell concentrator is well understood, developing the methods to do so has not been a trivial process. Over the past few years, several effective on-chip, cell-concentrating techniques have been developed based on a variety of mechanisms. For example, the hydrodynamic effect can be utilized to trap cells within certain shaped channels;[11–14] optical or optoelectronic tweezers are able to manipulate cells with high precision;[15–19] bulk or surface acoustic waves can trap cells in well-defined resonant cavities;[20–24] the electrokinetic effect can be exploited to generate electrical fields and transport particles to regions near the electrodes.[25–34] These techniques exhibit impressive on-chip, cell-concentrating capabilities; however, most of these techniques lack the ability to dynamically concentrate particles at any prescribed position and consequently form programmable, complex patterns (*i.e.*, as a programmable cell

[a]*Department of Chemical Engineering, The Pennsylvania State University, University Park, PA 16802, USA*
[b]*Department of Engineering Science and Mechanics, The Pennsylvania State University, University Park, PA 16802, USA. E-mail: junhuang@psu.edu; Fax: +1 814-865-9974; Tel: +1 814-863-4209*

† Electronic supplementary information (ESI) available. See DOI: 10.1039/c3lc00043e

‡ These authors contributed equally to this work.

concentrator). In this regard, it is essential to develop a programmable, biocompatible, on-chip cell concentrator.

The use of acoustically activated bubbles to trap particles shows great potential for realizing a programmable cell-concentrating technique. In such systems, acoustic waves (kHz range) oscillate the air–liquid interface of a bubble.[35–37] The oscillatory response is localized and confined to a region comparable with the radius of the bubble ($\sim$100 μm). It has been observed that particles located in this region can be trapped near the surface of the bubble due to an emergent acoustic radiation force.[38–40] Although bubble-based systems are able to locally trap particles in well-defined areas, difficulties exist in dynamically controlling the size and location of the bubbles. This limitation hinders the ability of such systems to concentrate cells in a programmable manner. Attentive solutions to this challenge involve the fabrication of cavities using lithography techniques.[41,42] This strategy enables researchers to control the size and location of the bubbles; however, once the cavities are prepared, the size and location of the bubble can no longer be changed. In this sense, the lithography-based method operates in a static manner.

In this article, we present an ''optoacoustic tweezers'' technique for dynamically concentrating particles/cells at any desired location within a microfluidic chamber and forming dynamic particle/cell patterns. This technique utilizes the opto-thermal effect[43–46] to generate bubbles[47] in a microchamber and acoustic radiation forces to trap particles/cells. By taking advantages of both opto-thermal bubble generation and acoustic-based trapping mechanism, the ''optoacoustic tweezers'' technique is capable of creating programmable, complex patterns in a biocompatible manner. It has the following advantages:

(a) Programmability: The size and location of the bubbles are controlled by the power and position of a diode laser, thus our technique is capable of generating bubbles at arbitrary locations in the microchamber without the use of permanent structures. Acoustic waves are then applied to the bubbles, enabling us to trap particles at any location in the microchamber.

(b) Localized cell-concentrating effect: The acoustic trapping force is local, rather than global, allowing us to trap particles/cells around the bubbles, while leaving others undisturbed. This local cell-trapping property, combined with the ability to create programmable, complex bubble arrays, can achieve flexible cell patterns of varying complexity. This cell-concentrating capability has not been previously demonstrated by any other methods.

(c) Biocompatibility: The bubble-based acoustic method operates at low power and thus is rather biocompatible. The laser only turns on during the bubble-generation process; it is off during the cell-concentrating process. Therefore, the ''optoacoustic tweezers'' technique is expected to be biocompatible, which is confirmed by the results from cell-adhesion tests.

(d) Simplicity: Unlike optical tweezers, our experimental setup does not require high-power laser or high-numerical-aperture lenses. All setups are easy-to-assemble and easy-to-operate.

With these advantages, it is expected that the ''optoacoustic tweezers'' technique presented here could be valuable in many applications[48–51] in engineering, chemistry, medicine, and physics.

Theory

When acoustic waves are applied to a bubble in liquid medium, the bubble oscillates and attracts cells to the surface of the bubble, achieving a biocompatible mechanism for locally concentrating cells. There are two forces exerted on cells when they are introduced into the flow field near an acoustically actuated bubble: drag force (F_d) and radiation force (F_r). In order to optimize the local cell-trapping effect, the amplitude of these two forces must be precisely controlled.

The drag force, a result of acoustic streaming, is exerted on the cells when they are injected into the acoustic flow field. Acoustic streaming[52,53,54] is generated by the non-uniform oscillation of the surface bubble; this oscillation causes the air–liquid interface to vibrate with different velocities, causing vortex-shaped streaming patterns. F_d acts opposite to the relative velocity of a cell in a fluid. The amplitude of F_d on a cell, approximated as a spherical particle here, is:

$$F_d = 6\pi\eta R_s v \quad (1)$$

where η is the viscosity of medium, R_s is the radius of the cell, and v is the relative velocity between cell and fluid. In eqn (1), since v is difficult to calculate at each position in the flow field, the upper-limit of F_d can be estimated using the maximum acoustic streaming velocity:

$$F_{d_{MAX}} = 6\pi\eta R_s U_L \quad (2)$$

$$U_L = \omega^{-1} u_0^2 R_p^4 r^{-5} \quad (3)$$

where $F_{d_{MAX}}$ is the upper-limit of drag force; U_L is the maximum acoustic streaming velocity; R_p is the radius of bubble; r is the distances between cells and bubble; $\omega = 2\pi f$, f is the oscillating frequency; and u_0 is the surface velocity of bubble, which is determined by the oscillatory frequency and amplitude.

The acoustic radiation force[55–59] is derived from the time-averaged, second-order momentum terms in the Navier–Stokes equation. Unlike the streaming effect, F_r can either attract cells towards the bubble or repel them from the bubble. The amplitude of F_r is described as below:[40]

$$F_r = \frac{4}{3}\pi R_s^3 d_m u_0^2 B R_p^4 r^{-5} \quad (4)$$

$$B = 3(d_s - d_m)/(2d_s + d_m) \quad (5)$$

where d_s is the density of cells, d_m is the density of medium, and B determines the direction of the acoustic radiation force

($B > 0$, particles are attracted to the bubble; $B < 0$, particles are repelled away from the bubble). Since cells have a higher density than the medium, they tend to be attracted to the bubble's surface.

The relative amplitudes of $F_{d_{MAX}}$ and F_r determine whether the cells' motion will be dictated by the drag force or the radiation force. To quantify this, the ratio between $F_{d_{MAX}}$ and F_r is described below:

$$\frac{F_{d_{MAX}}}{F_r} = \frac{9}{4}\frac{\eta}{\pi B d_m} f^{-1} R_s^{-2} \quad (6)$$

Eqn (6) shows that with higher oscillating frequency or relatively large cell size, F_r will play a more important role than F_d in the motion of the particles, causing the cells to be attracted to the bubble's surface. Otherwise, F_d will determine the trajectories of cells and they will follow the streaming pattern.

For a given device, η, B, and d_m in eqn (6) are constants. R_s is defined by the cells chosen to be concentrated. Therefore, optimizing f is vital for the performance of the device. However, choosing f is not trivial because bubbles can only be effectively actuated near certain resonant frequencies, which are tightly related to the bubble's size. The resonant frequencies for a spherical bubble at oscillating mode n are described as:[60]

$$f_n^2 \approx \frac{1}{4\pi^2}(n-1)(n+1)(n+2)\frac{\sigma}{d_m R_p^3} \quad (7)$$

where f_n is the resonant frequency at oscillation mode n and σ is the surface tension of medium. Optimizing device performance requires considering both eqn (6) and (7). An optimized f should be near the f_n for a bubble with radius R_p; at the same time, the value of f must keep $F_{d_{MAX}}/F_r$ smaller than 1, so that the radiation force will dictate particles' motion. This theory can predict the experimental condition for trapping cells near the acoustically activated bubbles; however, the effectiveness of acoustic operation is determined by the location and size of the bubble. In the next section, the opto-thermal effect is applied to generate highly controllable bubbles for acoustic cell trapping.

Experiments

Device setup

A schematic of the bubble-generation system is shown in Fig. 1a. A diode laser (wavelength of 405 nm) was coupled into an upright optical microscope (Eclipse LV-100, Nikon). The objective lens (10×, NA = 0.3) on the microscope was used to focus the diode laser as well as image the sample on a CCD camera (DS-Fi1, Nikon). The sample was a cell suspension which was contained in a glass chamber. The chamber was formed by separating two glass slides (top slide 25 × 25 mm, bottom slide 25 × 50 mm, VWR) with tape (Scotch Magic Tape). The resulting thickness of the chamber was about 70 μm. A gold film with 50 nm thickness was evaporated onto the top glass slide (Semicore evaporator). This film can absorb laser power and heat the surrounding water, resulting in the generation of surface bubbles. The laser was focused onto an area of approximately 1200 μm^2 on the gold film. The laser power, which was measured by a power meter (FieldMaxII-TO, Coherent) after the objective lens, was adjustable from 0 to 46 mW. Changing the location of the laser spot can be achieved by either moving the chamber in the xy plane or modulating the diode laser. In our experiment, a motorized stage was used to move the glass chamber and change the laser-focusing position. Once the cell suspension was injected into the chamber, the chamber was sealed with petroleum jelly (Equate). A piezo transducer (Model 273-073, RadioShack Corp.) was bonded to the bottom slide using epoxy and was used to generate acoustic waves. After surface bubbles were generated by the focused diode laser, the piezo transducer was actuated by a function generator (8116A, Hewlett Packard) at a frequency of ~100 kHz. This caused the surface bubbles to oscillate and allowed one to trap cells close to the bubbles.

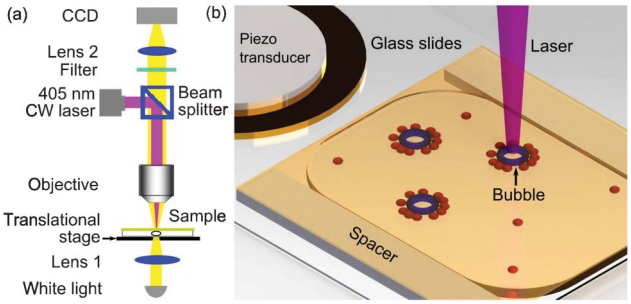

Fig. 1 Schematics of experimental setups. (a) The optical setup to generate surface bubbles *via* the opto-thermal effect. (b) Glass chamber to accommodate cell suspensions and micro-bubbles. The piezo transducer was used to generate acoustic waves.

Cell-adhesion test

HeLa cells were grown in Dulbecco's Modified Eagle Medium: Nutrient Mixture F-12 (DMEM/F12) media (Gibco, CA), supplemented with 10% fetal bovine serum (Atlanta Biologicals, GA), penicillin (100 U ml^{-1}), and 100 μg ml^{-1} streptomycin (Mediatech, VA), to about 90% confluence before trypsinization (Trypsin +0.05% EDTA, Gibco, CA). After centrifugation at 800 rpm for 5 min, cells were re-suspended in fresh medium or PBS buffer (1×, pH 7.4) to a final concentration of about 2×10^5 cells ml^{-1} for the experiment.

In the cell-adhesion experiment, the bottom glass slide was replaced by a cell culture slide (Thermanox). All other elements in the setup were left unchanged. About 10 μl of cell solution was added to the chamber. After the cells were concentrated at prescribed locations, the periphery of the platform was sealed with petroleum jelly to prevent evaporation, and the entire device was placed in a CO_2 incubator. Concentrated HeLa cells were cultured at 37 °C and 5% CO_2 for 2 h to assess the biocompatibility of this device by observing cell attachment.

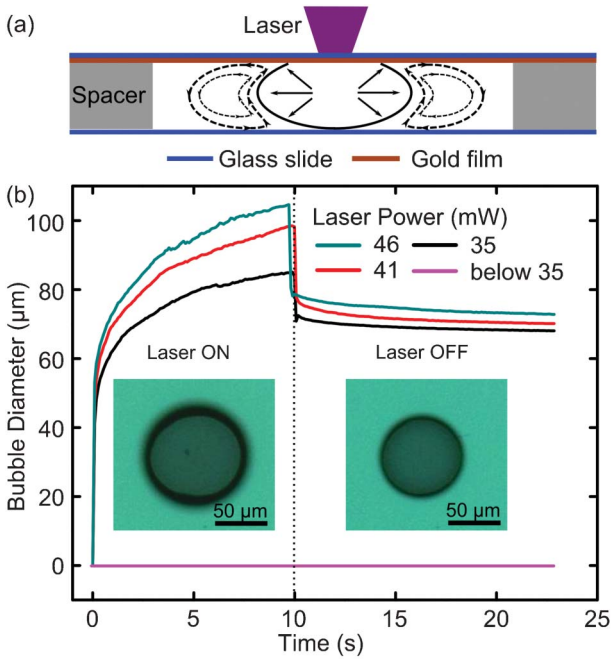

Fig. 2 (a) Schematics of the bubble-generation process. When the laser is focused on the gold film, the opto-thermal effect causes water to evaporate, and a bubble is generated in the micro-chamber. During this process, the heated water also causes convection flow in the chamber. (b) The bubble-expansion process with different levels of laser power. After the laser is turned off, the bubble exhibits a sudden decrease in size.

Results and discussion

Bubble generation using opto-thermal effect

In this experiment, the micro-bubble was generated by the laser-induced, opto-thermal effect. This method offers excellent control of the position and size of the micro-bubble, factors that play key roles in the trapping and patterning of cells. Fig. 2a demonstrates the mechanisms for bubble generation. When the diode laser (405 nm wavelength) is focused onto the gold film, the gold film absorbs energy from the laser and is rapidly heated. As a result, the water in contact with the gold film is also heated, and the convection flow is generated due to the heating effect (dashed lines in Fig. 2a). Above a certain laser power threshold, the water in the chamber reaches its boiling point, and a micro-bubble is generated at the interface of the gold film and the water inside the chamber. The laser power threshold in our experiment was about 35 mW. When incident laser power exceeded 35 mW, a micro-bubble was generated. Fig. 2b shows the size of the bubble both during and after the bubble-generation process. The bubble expands very fast when the laser is first turned on (0–40 μm diameter increase in the first 0.1 s). After this short time period, the rate of bubble expansion increases with increasing laser power. In 10 s, the bubble diameter can reach up to 100 μm using a 46 mW laser. During the bubble-generation process, the bubble stays in contact with the gold film; this allows the position of the surface bubble to remain stable. Stable positioning of the bubble is required in order to define a location for cell trapping.

In order to avoid possible heat damage to the cells during the experiment, the laser was turned off after the bubble-generation process. Upon removing the laser, it was observed that the bubble promptly shrunk in size due to the sudden temperature decrease (Fig. 2b). After the sudden shrink in size, the bubble's size (with diameter 60–80 μm) can remain stable for hours, which is long enough to perform cell manipulation. In addition, bubble diameters greater than 80 μm can be obtained if the laser is focused on the glass slide for a longer duration; however, the bubble size we used here (60–80 μm) is optimal for the following bubble-based acoustic cell trapping experiments. Optimizing these parameters is essential for the effective trapping of cells.

Bubble oscillation characterization

By successfully controlling the bubble's size with the laser, we were able to optimize R_p (30–33 μm) and f (about 100 kHz). The optimized f was approximately the same as the 5th harmonious resonant frequency of a 32 μm radius bubble (f_5 = 97.5 kHz). The vibration of the bubble's surface was detected by a fast camera (Fastcam SA4, Photron) at 225 000 fps. Fig. 3a and 3b show the oscillation of the bubble at 100 kHz using an acoustic wave with amplitude of 10 V peak-to-peak (Vpp). The bubble oscillates near the 5th harmonious mode as predicted. The oscillation amplitude was measured by recording the position change of the arrow-indicated point in Fig. 3b, which is about 2 μm (Fig. 3c). Surface velocity (u_0) was calculated by the period and amplitude from Fig. 3c, which is about 0.8 m s^{-1}.

When operating with HeLa cells (R_s=10 μm), the calculated F_r (by eqn (4)) at different r are displayed in Fig. 3d. F_r increases drastically when cells get near the bubble, which indicates that the trapping of cells to the bubble surface is stable. The ratio between the $F_{d_{MAX}}$ and F_r is also illustrated in Fig. 3e. When the radiation force is larger than the maximum drag force, we can expect that HeLa cells will move toward the bubble's surface under experimental conditions. The following cell-trapping experiment verifies this theoretical calculation.

Locally concentrating HeLa cells

HeLa cells were used to test the cell-concentrating performance of the device. The acoustic parameters used followed the calculated frequency (100 kHz) and amplitude (10 Vpp). Initially, HeLa cells were distributed randomly throughout the chamber (Fig. 4a); after turning on the acoustic waves, it was observed that cells moved towards the bubble's surface and aggregated there (Fig. 4b) within 20 s. After the cells had aggregated, the acoustic waves were turned off, and cells were found to be concentrated within 100 μm of the bubble's center. It should be noted that the concentrating effect was local, meaning that only the cells near the bubble (distance within about 500 μm), rather than all of the cells in the chamber, were trapped at the bubble's surface.

The cell-concentrating process was further investigated quantitatively. Two parameters were used to evaluate the device's cell-concentrating performance: (1) Average distance between cells was used to describe how cells aggregate with each other. Before the bubble was actuated, this value was about 246.4 ± 49.97 μm. After the bubble was actuated, this

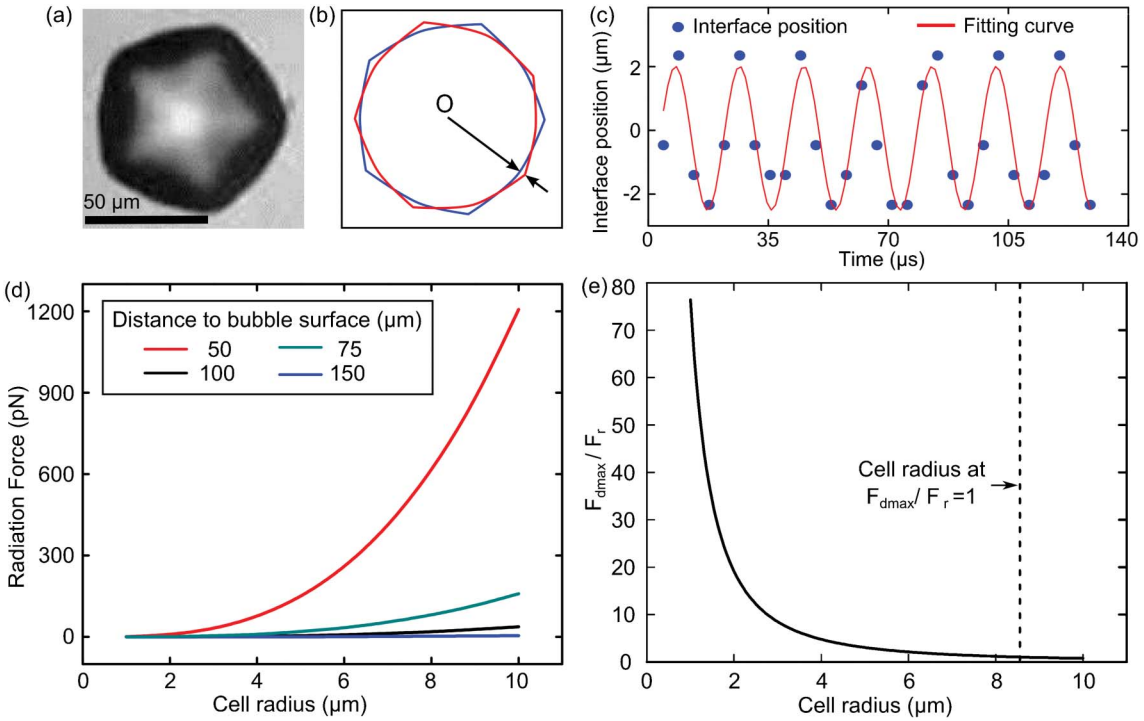

Fig. 3 (a) The bubble with a radius of 32 μm oscillates at the 5th harmonious mode at 100 kHz. (b) The bubble oscillates between the statuses represented by blue and red lines. The arrow indicates the point used to measure the oscillating amplitude. (c) The change in position of bubble's surface (arrow in (b)), the bubble oscillates at the same frequency as the stimulating acoustic waves with an amplitude of 2 μm; the surface velocity was calculated as 0.8 m s^{-1}. (d) The amplitude of acoustic radiation force. (e) The ratio between maximum drag force and radiation force.

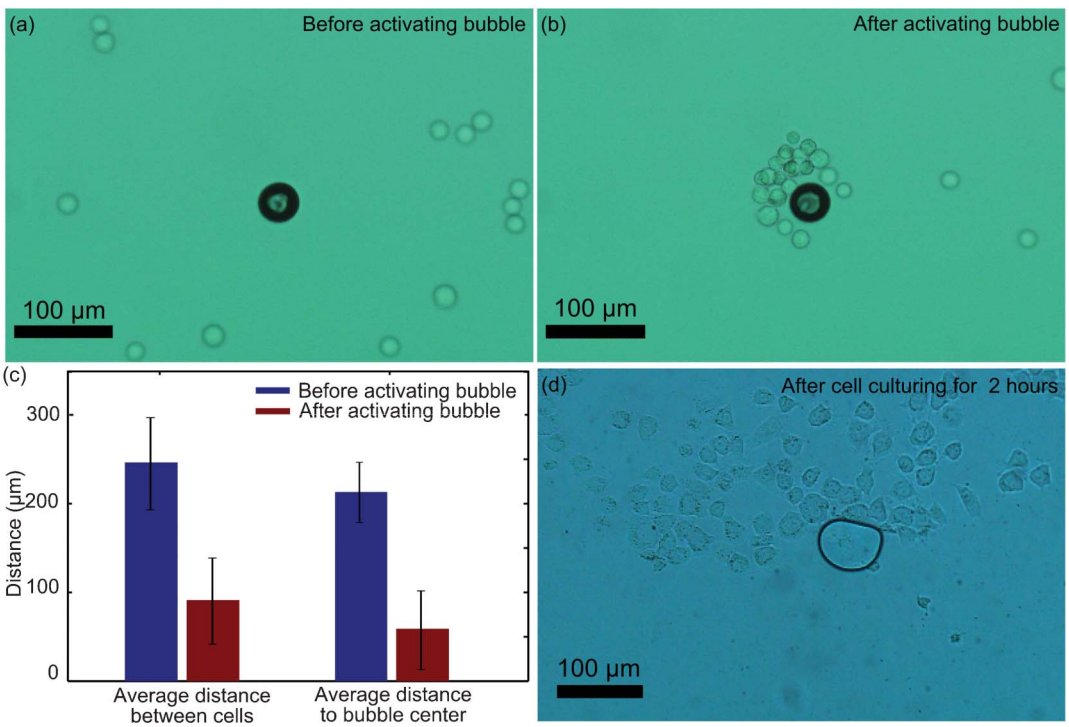

Fig. 4 (a) HeLa cells distribute randomly throughout the chamber before bubble actuation. (b) HeLa cells move and aggregate near the bubble's surface after bubble actuation. (c) Statistics show that cells aggregate both with each other and close to the bubble's center. (d) Cell-adhesion test results show all cells are attached to the culturing slides, indicating that our approach has good biocompatibility.

value decreased to 91.26 ± 54.96 μm, indicating that cells came closer due to the oscillation of the bubble. (2) The average distance from cells to the bubble's center was used to evaluate the extent to which the device is able to trap cells near the bubble. This value changed from 212.9 ± 29.99 μm to 58.87 ± 45.35 μm after acoustic treatments. Considering that the bubble has a radius of 30 μm, this value indicates that the cells were trapped very close to the bubble's surface. Another experiment with a mixture of Hela cells (radius: ~10 μm) and yeast (radius: ~2.5 μm) showed that the movement of Hela cells is dominated by the radiation force, because the ratio of $F_{d_{MAX}}/F_r$ is smaller than 1. As a result, they are more easily trapped near the bubble's surface. On the contrary, the movement of yeast cells is dominated by the drag force, and they tend to follow the streaming lines around the bubbles under the same operation parameters (Fig. S1, ESI†). This phenomenon confirmed the prediction from our theory that the value of $F_{d_{MAX}}/F_r$ increases as the radius of particles/cells decreases.

Cell-adhesion tests were also conducted to confirm the biocompatibility of this system. In such experiments, the cell-culturing slides replaced the commonly used glass slides and all other elements were left unchanged. After the cells were concentrated, they were cultured for 2 h and allowed to attach onto the slides. Fig. 4d shows the cell-culturing results. It was observed that all of the cells in the microscope's vision adhered to the cell-culturing slides and were kept alive after the bubble was activated acoustically. The results indicate: (1) Laser heat should be non-invasive towards the cells in this experiment because the laser is focused on the gold film, rather than directly on the cells, and the laser is turned off once the cell-concentrating process starts. (2) Compared with the acoustic methods for ultrasound-mediated drug delivery,[61,62] sonoporation and sonolysis,[63] our bubble-based acoustic technique operates at a much lower acoustic power, thus avoiding potential damage to cells. (3) The generated bubble is extremely small compared with the total area of the microchamber, and most cells do not attach directly to the bubble's surface. Therefore, the generated bubble has little disturbance on cells' living environments. Overall, this technique is demonstrated to be biocompatible and suitable for cell-related studies and applications.

Programmable particle/cell concentrating

Our technique's ability to concentrate particles/cells at multiple positions was examined on both polystyrene particles (15 μm in diameters) and HeLa cells. In Fig. 5a and 5b, surface bubbles were generated in pre-defined patterns (two bubbles in a line for Fig. 5a, and a square with a bubble in the center for Fig. 5b). When acoustic waves were applied, polystyrene particles were trapped near each bubble's surface. This resulted in the patterning of the particles/cells that closely resembled the well-defined bubble array. The distance between each aggregation of particles was approximately equal to the distance (~200 μm) between bubbles. We further proved that this optoacoustic tweezers method can be readily used to form pre-defined patterns of cells. As an example, triangle (Fig. 5c) and centered triangle patterns (Fig. 5d),

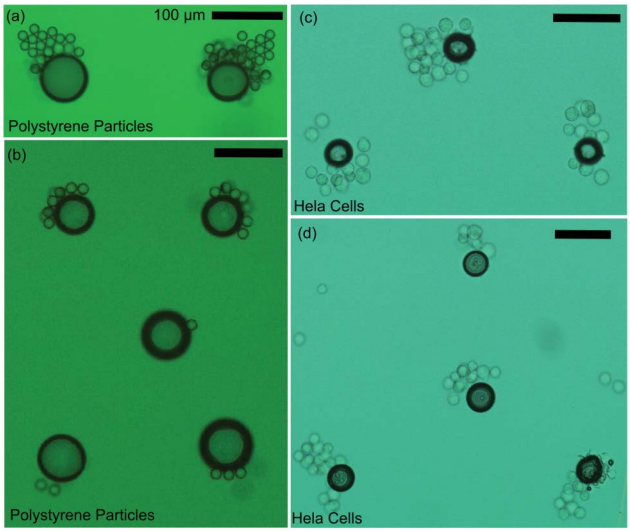

Fig. 5 Patterns of particles and cells generated by optoacoustic tweezers. (a, b) Patterning of polystyrene particles with 15 μm diameters. (c, d) Patterning of HeLa cells with about 20 μm diameters. The scale bar represents 100 μm.

which are usually difficult to obtain by other cell-patterning mechanisms, were achieved.

The formation of complex, dynamic patterns relies on two unique characteristics of our device: the ability to generate well controlled bubbles at any location in the microchamber; and the capacity to locally, rather than globally, trap particles/cells near the generated bubbles. Precise control over the size and location of the generated bubbles allows us to form any desired pattern, and the local trapping effect enables us to pattern target cells at each of these locations, while leaving others undisturbed. In the experiment, we also found that acoustic power and exerting time influenced the pattern. Higher acoustic power caused a larger acoustic radiation force, resulting in the trapping of more cells near the bubble; longer working times permitted more cells to aggregate near the bubble surface. Overall, the optoacoustic tweezers method shows great potential in concentrating cells in a programmable, biocompatible manner.

Conclusion

In summary, we have integrated an acoustic-based cell trapping mechanism with an opto-thermal bubble generation method in order to develop a simple, effective, programmable, biocompatible approach for concentrating cells locally in a microfluidic chamber. This device features several unique advantages: (1) The size and location of opto-thermally generated surface bubbles can be dynamically controlled by changing the power and position of a laser focused on a gold film. Strong acoustic radiation forces (larger than 100 pN) can be exerted on nearby cells by applying acoustic waves to the surface bubble array. By combining these two effects, this method can effectively collect cells at any prescribed position in the chamber. (2) This device has great biocompatibility.

HeLa cells were trapped effectively in a region extending no further than 100 μm from the center of the bubble. The cells were successfully attached to a culturing slide and were kept alive after the trapping process.

In the future, this device is expected to be further improved in several aspects. Spatial light modulators can be used to modulate the diode laser. In this manner, more complicated surface bubble patterns can be achieved simultaneously, which can further improve the functionalities of this device. Moreover, there is still a great deal of room to miniaturize the entire setup. For example, a blue-ray DVD laser head, including the laser source and focusing lens, can be integrated with a microfluidic channel to replace the bulky optical microscopy unit. Overall, advantages such as programmability, biocompatibility, and ease-of-fabrication/use render the optoacoustic tweezers method presented here desirable for a variety of applications, including bio-sensing, cell microarrays, cell analysis, and tissue engineering.

Acknowledgements

The authors thank Matt Jaffe and Jason Scott for their helpful discussion. This research was supported by National Institutes of Health (Director's New Innovator Award, 1DP2OD007209-01), National Science Foundation, and the Penn State Center for Nanoscale Science (MRSEC) under grant DMR-0820404. Components of this work were conducted at the Penn State node of the NSF-funded National Nanotechnology Infrastructure Network.

References

1 D. Irimia and M. Toner, *Lab Chip*, 2006, **6**, 345–352.
2 M. Yamada and M. Seki, *Lab Chip*, 2005, **5**, 1233–1239.
3 C. J. Flaim, S. Chien and S. N. Bhatia, *Nat. Methods*, 2005, **2**, 119–125.
4 P. Bajaj, D. Marchwiany, C. Duarte and R. Bashir, *Adv. Healthcare Mater.*, 2013, **2**, 450–458.
5 M. M. Stevens, M. Mayer, D. G. Anderson, D. B. Weibel, G. M. Whitesides and R. Langer, *Biomaterials*, 2005, **26**, 7636–7641.
6 C. Smith, *Nature*, 2007, **446**, 219–222.
7 S. Park, X. Hong, W. S. Choi and T. Kim, *Lab Chip*, 2012, **12**, 3914–3922.
8 X. Tang, P. Bajaj, R. Bashir and T. Saif, *Soft Matter*, 2011, **7**, 6151–6158.
9 P. A. Belter, E. L. Cussler and W.-S. Hu, In *Bioseparations: Downstream Processing for Biotechnology*, Wiley, New York, 1988.
10 M. G. P. Stoker and H. Rubin, *Nature*, 1967, **215**, 171–172.
11 S. Park, D. Kim, R. J. Mitchell and T. Kim, *Lab Chip*, 2011, **11**, 2916–2923.
12 L. Zhu, Q. Zhang, H. Feng, S. Ang, F. S. Chau and W.-T. Liu, *Lab Chip*, 2004, **4**, 337–341.
13 J. Sun, M. Li, C. Liu, Y. Zhang, D. Liu, W. Liu, G. Hu and X. Jiang, *Lab Chip*, 2012, **12**, 3952–3960.
14 A. J. Mach, J. H. Kim, A. Arshi, S. C. Hur and D. D. Carlo, *Lab Chip*, 2011, **11**, 2827–2834.
15 H.-Y. Hsu, A. T. Ohta, P.-Y. Chiou, A. Jamshidi, S. L. Neale and M. C. Wu, *Lab Chip*, 2010, **10**, 165–172.
16 H. Hwang and J.-K. Park, *Lab Chip*, 2009, **9**, 199–206.
17 B. S. Schmidt, A. H. J. Yang, D. Erickson and M. Lipson, *Opt. Express*, 2007, **15**, 14322–14334.
18 H. Hwang, Y.-H. Park and J.-K. Park, *Langmuir*, 2009, **25**, 6010–6014.
19 C. Escobedo, A. G. Brolo, R. Gordon and D. Sinton, *Nano Lett.*, 2012, **12**, 1592–1596.
20 M. K. Tan, J. R. Friend and L. Y. Yeo, *Lab Chip*, 2007, **7**, 618–625.
21 J. Shi, D. Ahmed, X. Mao, S.-C. S. Lin, A. Lawit and T. J. Huang, *Lab Chip*, 2009, **9**, 2890–2895.
22 X. Ding, J. Shi, S.-C. S. Lin, S. Yazdi, B. Kiraly and T. J. Huang, *Lab Chip*, 2012, **12**, 2491–2497.
23 X. Ding, S. S. Lin, B. Kiraly, H. Yue, S. Li, I.-K. Chiang, J. Shi, S. J. Benkovic and T. J. Huang, *Proc. Natl. Acad. Sci. U. S. A.*, 2012, **109**, 11105–11109.
24 B. Hammarström, M. Evander, H. Barbeau, M. Bruzelius, J. Larsson, T. Laurell and J. Nilsson, *Lab Chip*, 2010, **10**, 2251–2257.
25 P. K. Wong, C.-Y. Chen, T.-H. Wang and C.-M. Ho, *Anal. Chem.*, 2004, **76**, 6908–6914.
26 L. Yang, P. P. Banada, M. R. Chatni, K. S. Lim, A. K. Bhunia, M. Ladisch and R. Bashir, *Lab Chip*, 2006, **6**, 896–905.
27 S. Park, Y. Zhang, T.-H. Wang and S. Yang, *Lab Chip*, 2011, **11**, 2893–2900.
28 S. K. Cho, Y. Zhao and C.-J. Kim, *Lab Chip*, 2007, **7**, 490–498.
29 D. Puchberger-Enengl, S. Podszun, H. Heinz, C. Hermann, P. Vulto and G. A. Urban, *Biomicrofluidics*, 2011, **5**, 044111.
30 A. K. Balasubramanian, K. A. Soni, A. Beskok and S. D. Pillai, *Lab Chip*, 2007, **7**, 1315–1321.
31 C. R. Cabrera and P. Yager, *Electrophoresis*, 2001, **22**, 355–62.
32 R. Kwak, S. J. Kim and J. Han, *Anal. Chem.*, 2011, **83**, 7348–7355.
33 B. Scarff, C. Escobedo and D. Sinton, *Lab Chip*, 2011, **11**, 1102–1109.
34 J. Gao, R. Riahi, M. L. Y. Sin, S. Zhang and P. K. Wong, *Analyst*, 2012, **137**, 5215–5221.
35 Y. Xie, D. Ahmed, M. Lapsley, S. S.-C. Lin, A. A. Nawaz, L. Wang and T. J. Huang, *Anal. Chem.*, 2012, **84**, 7495–7501.
36 D. Ahmed, X. Mao, B. K. Juluri and T. J. Huang, *Microfluid. Nanofluid.*, 2009, **7**, 727–731.
37 D. Ahmed, X. Mao, J. Shi, B. K. Juluri and T. J. Huang, *Lab Chip*, 2009, **9**, 2738–2741.
38 P. Rogers and A. Neild, *Lab Chip*, 2011, **11**, 3710–3715.
39 M. V. Patel, A. R. Tovara and A. P. Lee, *Lab Chip*, 2012, **12**, 139–145.
40 D. L. Miller, *J. Acoust. Soc. Am.*, 1988, **84**, 1378–1387.
41 C. Wang, S. V. Jalikop and S. Hilgenfeldt, *Appl. Phys. Lett.*, 2011, **99**, 034101–03.
42 C. Wang, S. V. Jalikop and S. Hilgenfeldt, *Biomicrofluidics*, 2012, **6**, 012801–11.
43 Y. Zheng, H. Liu, Y. Wang, C. Zhu, S. Wang, J. Cao and S. Zhu, *Lab Chip*, 2011, **11**, 3816–3820.
44 K. Zhang, A. Jian, X. Zhang, Y. Wang, Z. Li and H.-Y. Tam, *Lab Chip*, 2011, **11**, 1389–1395.

45 L. Jiang and D. Erickson, *Langmuir*, 2011, **27**, 11259–11264.
46 S. Park, T.-H. Wu, Y. Chen, M. A.Teitell and P. Y. Chiou, *Lab Chip*, 2011, **11**, 1010–1012.
47 X. L. Mao, B. K. Juluri, M. I. Lapsley, Z. S. Stratton and T. J. Huang, *Microfluid. Nanofluid.*, 2009, **8**, 139–144.
48 A. Arora, G. Simone, G. Salieb-Beugelaar, J. T. Kim and A. Manz, *Anal. Chem.*, 2010, **82**, 4830–4847.
49 P. Neuzil, S. Giselbrecht, K. Länge, T. J. Huang and A. Manz, *Nat. Rev. Drug Discovery*, 2012, **11**, 620–632.
50 S. Yang, F. Guo, B. Kiraly, X. Mao, M. Lu and T. J. Huang, *Lab Chip*, 2012, **12**, 2097–2102.
51 X. Mao and T. J. Huang, *Lab Chip*, 2012, **12**, 1412–1416.
52 W. L. Nyborg, *J. Acoust. Soc. Am.*, 1958, **30**, 329–339.
53 A. Prosperetti, *Ultrasonics*, 1984, **22**, 69–77.
54 D. Ahmed, C. Y. Chan, S. S. C. Lin, H. S. Muddana, N. Nama, S. J. Benkovic and T. J. Huang, *Lab Chip*, 2013, **13**, 328–331.
55 X. Ding, S. C. S. Lin, M. I. Lapsley, S. Li, X. Guo, C. Y. K. Chan, I. Chiang, J. P. McCoy and T. J. Huang, *Lab Chip*, 2012, **12**, 4228–4231.
56 S. C. S. Lin, X. Mao and T. J. Huang, *Lab Chip*, 2012, **12**, 2766–2770.
57 J. Shi, S. Yazdi, S. C. S. Lin, X. Ding, I. Chiang, K. Sharp and T. J. Huang, *Lab Chip*, 2011, **11**, 2319–2324.
58 J. Shi, H. Huang, Z. Stratton, A. Lawit, Y. Huang and T. J. Huang, *Lab Chip*, 2009, **9**, 3354–3359.
59 J. Shi, X. Mao, D. Ahmed, A. Colletti and T. J. Huang, *Lab Chip*, 2008, **8**, 221–223.
60 T. G. Leighton, *The Acoustic Bubble*, Elsevier, 1994.
61 M. D. Sherar, M. B. Noss and F. S. Foster, *Nature*, 1987, **330**, 493–495.
62 S. Mitragotri, D. Blankschtein and R. Langer, *Science*, 1995, **269**, 850–853.
63 T. Tandiono, D. S. Ow, L. Driessen, C. S. Chin, E. Klaseboer, A. B. Choo, S. W. Ohl and C. D. Ohl, *Lab Chip*, 2012, **12**, 780–786.